COMPARISON OF EFFICIENT UNCERTAINTY QUANTIFICATION TECHNIQUES ON A TRANSONIC AIRFOIL, USING RANS COMPUTATIONS AND ADJOINT METHOD

Q. Bennehard[1], J. Peter[2], and M. Carini[2]

[1,3] ONERA, Université Paris-Saclay, F-92190 Meudon, France
e-mail: quentin.bennehard@onera.fr, marco.carini@onera.fr

[2] ONERA, Université Paris-Saclay, F-92322 Châtillon, France
jacques.peter@onera.fr

Abstract

This paper presents a comparison among efficient techniques for uncertainty quantification on the RAE2822 airfoil whose shape is affected by uncertain geometrical parameters. Transonic conditions are considered with focus on estimating the statistics of the aerodynamic coefficients predicted by RANS simulations and using a far-field drag analysis of the computed flow field. Generalized polynomial chaos expansion with least-square approximation is employed for stochastic surrogate modelling. Two different kind of approaches enabling the high-dimensionality of the uncertainty space are investigated: 'compressed sensing' through Least Angle Regression and Basis Pursuit Denoising methods, and the 'gradient enhanced' formulation of the least-square approach exploiting the adjoint capabilities of modern CFD solvers.

Keywords: transonic airfoil, CFD, geometric uncertainty, polynomial chaos, compressed sensing, adjoint gradient-enhancement.

1 INTRODUCTION

During the last decades, computing power has largely increased, contributing to make Computational Fluid Dynamics (CFD) a quite mature tool for industrial design, widely exploited for various applications, especially in the aeronautical sector. However, the awareness of discrepancies between the ideal conditions of numerical simulations and the real ones has motivated the increasing attention towards sensitivities of classical optimal shapes to uncertain parameters robust design techniques [9] and robust design techniques [10].

These uncertainties are usually of two kinds: epistemic and aleatory. The first one originates in our lack of knowledge in the modelling of the physical phenomena. In this context, Uncertainty Quantification (UQ) can help making our physical models more reliable. The second type is related to the variability in shape or flow conditions and although it cannot be controlled, it still needs to be considered in the design process. For example, deviations of real aerodynamic shapes from their reference design are often encountered, not only due to manufacturing tolerances but also to temporary and permanent degradation of aerodynamic surfaces along their lifespan.

Consequently, to be able to provide a robust aerodynamic shape by numerical optimization, uncertainties must be integrated in the design process. The state of the art of shape optimization provides, with the adjoint approach, the capability to tackle high dimensional design space [11]. However, on the other hand, the number of uncertain inputs can also become significantly large and, today, for such complex cases treated with High-Fidelity (HiFi) CFD, designers are struggling with what is known as the "curse of dimensionality". This curse represents the main bottleneck for the widespread application of UQ techniques in the industrial framework.

The main focus of this paper will be on efficient polynomial chaos techniques which can afford a reduced number of expensive CFD computations: compressed sensing (Least Angle Regression [3], Basis Pursuit Denoising [12]) and adjoint-gradient enhanced variants [8], [9] of the standard least-square approximation. Their implementation will mainly rely on the functionalities already available in the open-source toolboxes *OpenTURNS* [5] (http://openturns.github.io/) and *eQuadrature* [4] (https://equadratures.org/). These techniques will be compared on the a realistic design test case represented by a transonic airfoil whose shape design parameters are considered uncertain with focus on efficiently estimating the statistics associated with its aerodynamic coefficients.

2 METHODOLOGY

Polynomial Chaos Expansion is a well establish approach [1] to derive a surrogate model approximating a function of interest $f(\boldsymbol{x})$ in the form of multivariate polynomials $H_j(\boldsymbol{x})$:

$$f(\boldsymbol{x}) = \sum_{\boldsymbol{j}}^{\infty} c_{\boldsymbol{j}} H_{\boldsymbol{j}}(\boldsymbol{x}), \tag{1}$$

where $\boldsymbol{x}$ is a d-dimensional vector of independent random variables, $\boldsymbol{j}$ the multi-index associated with univariate polynomials and $c_{\boldsymbol{j}}$ the polynomial coefficients. The polynomial expansion $\left\{H_j(x)\right\}_{j=0}^{\infty}$ is chosen as a complete orthogonal basis with respect to the inner product associated with the joint Probability Density Function (PDF) of $\boldsymbol{x}$, $\rho(\boldsymbol{x})$:

$$\langle H_{\boldsymbol{j}}, H_{\boldsymbol{k}} \rangle = \int H_{\boldsymbol{j}}(\boldsymbol{x}) \, \rho(\boldsymbol{x}) H_{\boldsymbol{k}}(\boldsymbol{x}) = \delta_{\boldsymbol{j},\boldsymbol{k}}, \tag{2}$$

with $(\boldsymbol{x}) = \prod_{i=1}^{d} \rho_i(x_i)$, $\rho_i(x_i)$ being the marginal probability density function characterizing the ith uncertain variable x_i. Different truncation rules, e.g. total order or a hyperbolic cross [1], can be applied to Eq. (1), resulting in a different definition of the multi-index set J spanned by $\boldsymbol{j}$:

$$f(\boldsymbol{x}) = \sum_{j}^{J} c_j H_j(\boldsymbol{x}). \tag{3}$$

In the present paper, the total order rule is adopted by fixing a common maximum degree p for all the polynomial terms:

$$|\boldsymbol{j}| = \sum_{i=1}^{d} j_i \le p, \tag{4}$$

which leads to a total number n of polynomial terms (and hence of coefficients) to be determined given by n = (p + d)!/(p! d!). The PCE coefficients can be computed by various methods. In particular, when considering non-intrusive techniques, the different approaches can be essentially divided into two families: i) *Spectral projection methods*, where the coefficients are computed by the numerical approximation of the projection of $f(\boldsymbol{x})$ on the orthogonal polynomial basis using classical Gauss quadrature and their more efficient sparse versions [13]. ii) *Collocation methods*, where the PCE coefficients are computed by fitting Eq. (1) to a given number of collocation points in the uncertain space, to best reproduce the exact function value:

$$\begin{bmatrix} H_0(\boldsymbol{x}_1) & \dots & H_n(\boldsymbol{x}_1) \\ \vdots & \ddots & \vdots \\ H_0(\boldsymbol{x}_N) & \cdots & H_n(\boldsymbol{x}_N) \end{bmatrix} \begin{pmatrix} c_0 \\ \vdots \\ c_n \end{pmatrix} = \begin{pmatrix} f(\boldsymbol{x}_1) \\ \vdots \\ f(\boldsymbol{x}_N) \end{pmatrix}, \tag{5}$$

that can be written as $A\boldsymbol{c} = \boldsymbol{b}$ in compact form. Oversampling up to *2n* is often employed to satisfy the full-rank condition for the above matrix, resulting in a classical Least Square Approximation (LSA) of the PCE solution. This is equivalent to seek an approximation for the PCE coefficients in the form of an l_2-minimization problem:

$$\boldsymbol{c} = argmin \, \|A\boldsymbol{c} - \boldsymbol{b}\|_2. \tag{6}$$

2.1 Gradient-enhanced LSA

When gradient information is available, it can be used to introduce additional equations for the considered collations points while reducing their number in order to achieve full rank. In this case, the LSA system in Eq. (6) assumes the following form:

$$\begin{bmatrix} A^{(0)} \\ \vdots \\ A^{(d)} \end{bmatrix} \begin{pmatrix} c_0 \\ \vdots \\ c_n \end{pmatrix} = \begin{pmatrix} \boldsymbol{b}^{(0)} \\ \vdots \\ \boldsymbol{b}^{(d)} \end{pmatrix}, \tag{7}$$

with:

$$A^{(j)} = \begin{bmatrix} H_0^{(j)}(\boldsymbol{x}_1) & \cdots & H_n^{(j)}(\boldsymbol{x}_N) \\ \vdots & \ddots & \vdots \\ H_0^{(j)}(\boldsymbol{x}_1) & \cdots & H_n^{(j)}(\boldsymbol{x}_{N\ldots}) \end{bmatrix}, \qquad \boldsymbol{b}^{(j)} = \begin{pmatrix} f^{(j)}(\boldsymbol{x}_1) \\ \vdots \\ f^{(j)}(\boldsymbol{x}_N) \end{pmatrix}, \tag{8}$$

Where $A^{(0)} = A$ and $A^{(0)} = A$ $H_k^{(j)} = \partial H_k / \partial x_j$ for $j \geq 1$ $j \geq 1$. Since the gradient at each collocation point provides d additional scalar information, the total number of samples can be ideally reduced by the same factor with respect to the standard LSA formulation. However, attention has to be paid to accuracy issues in computing the derivative information, as often occurs for adjoint solvers employed in CFD applications. In order to reduce the sensitivity from numerical noise affecting the gradient accuracy, a null-space method has been proposed in [2] showing how this approach can achieve improved accuracy, especially for standard deviation, on a turbomachinery test case. The same method as implemented in the *eQuadratures* toolbox is employed here to compute the solution of the Gradient-Enhanced LSA problem (LSA-GE) presented in Eq. (7).

2.2 Compressed sensing techniques

When dealing with very limited amount of data (e.g. as a direct consequence of expensive function evaluations) resulting in an underdetermined system for Eq. (1), an alternative solution can be sought in a sparse form, i.e. by minimizing the number of non-zero entries of $\boldsymbol{c}$:

$$\boldsymbol{c} = argmin \, \|\boldsymbol{c}\|_0 \quad such \, that \quad \|A\boldsymbol{c} - \boldsymbol{b}\|_2 \leq \varepsilon, \tag{9}$$

where $\varepsilon \geq 0$ is a given tolerance on the interpolation condition and $\|\boldsymbol{c}\|_0$ denotes the l_0 norm of $\boldsymbol{c}$. Indeed, although real PCE models are not truly sparse, they are expected to be *compressible,* i.e. to feature a rapid decay in the magnitude of the coefficients at increasing order of the expansion, with most of the variance being captured by a few terms. This provides the rational behind the compressed sensing approach. Unfortunately, the cost of solving Eq. (9) grows exponentially with d and a convex relaxation based on l_1-minimization is often considered in practice. When $\varepsilon = 0$ this is also referred to as Basis Pursuit Denoising (BPDN) which leads to solve the following problem:

$$\boldsymbol{c} = argmin \, \|\boldsymbol{c}\|_1 \quad such \, that \quad \|A\boldsymbol{c} - \boldsymbol{b}\|_2 = 0, \tag{10}$$

using convex optimization algorithm. Besides convex optimization solvers, greedy methods have also been proposed to find a sparse PCE solution [1]. In these methods regressors are added to the model one by one according to some selection criterion, to find a heuristic solution to the burdensome l_0 minimization problem. An example is represented by LARS [3] where the regressors are added according to their correlation with the current residual and the PCE coefficients are then updated using a least angle strategy. It should be noted that LARS with the LASSO (Least Absolute Shrinkage and Selection Operator) modification can be interpreted as a l_1-optimization solver. Both techniques, BPDN and LARS will be considered in the present study. In particular, for LARS, the implementation available in the open-source library *OpenTURNS* [5] is employed.

3   THE RAE2822 TEST CASE

The considered test case is represented by the compressible viscous flow around the RAE2822 airfoil at transonic conditions: Mach number of 0.725, Reynolds number of 6.5e6,

and angle of attack of 2.55°: these conditions corresponds to the AGARD test case 7 [15]. The RANS solution is computed by using the *elsA* software [6] (ONERA-SAFRAN property) on a structured grid with a CH topology featuring a total of ~8e5 cells and near-wall resolution of $y^+ \sim 1.0$. The CFD solution is converged down to 7 orders of magnitude in the decrease of the residual. The employed mesh and the computed Mach field are illustrated in Figure 1.
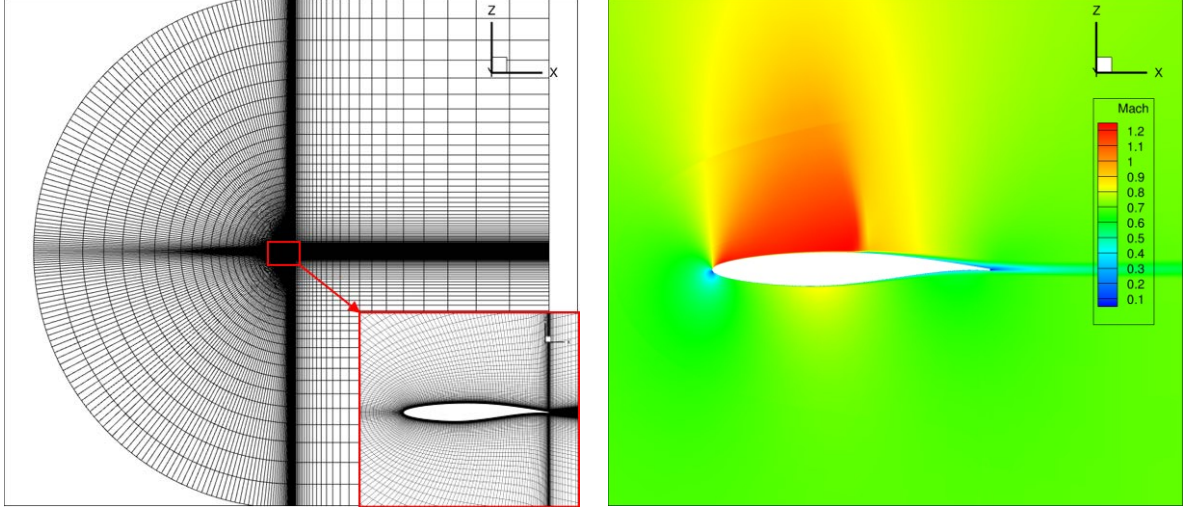

Figure 1: Computed Mach field for the transonic flow around the RAE2822 (right) and employed structured mesh (left).

A far-field drag analysis [7] is applied to CFD results in order to extract the different phenomenological sources of drag. In particular, the far-field estimation of the total drag coefficient CD_{ff} and the wave drag coefficient, CD_w, are considered as Quantity of Interest (QoI) for the present UQ analysis, in addition to the lift, CL, and pitching moment, CM_y, coefficients. Corresponding values for the reference airfoil geometry and the considered flight conditions are reported in Table 1.

CL	CD_{ff}	CD_w	CM_y
0.8076	139.37	24.20	-0.09465

Table 1: Computed values of the aerodynamic coefficients for the RAE2822 airfoil at considered transonic conditions. Drag coefficient values are reported in drag counts.

3.1 Uncertain shape parameterization

The airfoil shape is parameterized by means of both camber and thickness parameters at five different positions uniformly distributed along the chord, i.e. at 16.7%, 33.3%, 50%, 66.7%, 83.3%, as illustrated in Figure 2. The deviation of each parameter from its corresponding baseline value is assumed to follow a zero-mean β distribution. The convention used to define the probability density function of the β distribution is recalled Eq. (11):

$$f_X(x) = \frac{(x-a)^{\alpha-1}(b-x)^{\beta-1}}{(b-a)^{\alpha+\beta-1}B(\alpha,\beta)} \qquad \text{with } x \in [a,b] \text{ and } B \text{ being the Euler's β function} \qquad (11)$$

For all camber parameters the same value of variance is employed. The same assumption applies to the thickness parameters. Two different levels of amplitude, namely Ω_1 and Ω_2 are

considered for the uncertain perturbations: the associated sets of β-PDF parameters are reported in Table 2, while a representation of the envelope of the resulting airfoil shape is illustrated in Figure 3 and Figure 4 for Ω_1 and Ω_2 cases, respectively. Not surprisingly, the envelope is wider for Ω_2 and as a consequence, the pressure coefficient distribution shows quite large deviations from the reference results, especially affecting the shock position on the suction side of the airfoil, as illustrated in Figure 4. For each realization of the uncertain design parameters, a mesh deformation process is used to adapt the baseline airfoil mesh and re-run CFD computations for both primal and adjoint analysis.
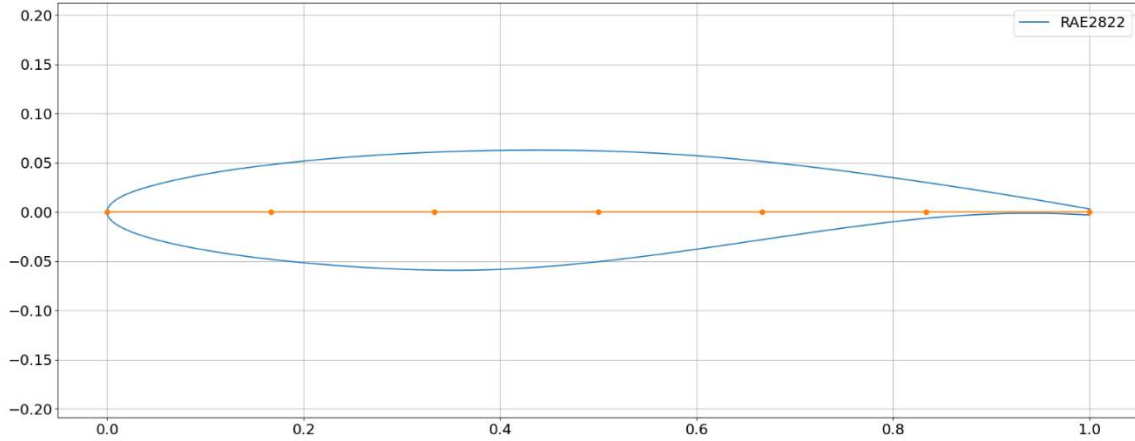

Figure 2: RAE2822 baseline airfoil geometry (light blue line) and position of the control points used to modify the camber and thickness laws (orange makers and line).

		standard deviation	shape parameter $\alpha=\beta$	lower bound (a)	upper bound (b)
Ω_1	camber	0.5E-3	4	-1.5E-3	+1.5E-3
	thickness	1.0E-2	4	-3.0E-2	+3.0E-2
Ω_2	camber	3.0E-3	4	-9.0E-3	+9.0E-3
	thickness	6.0E-2	4	-18.0E-2	+18.0E-2

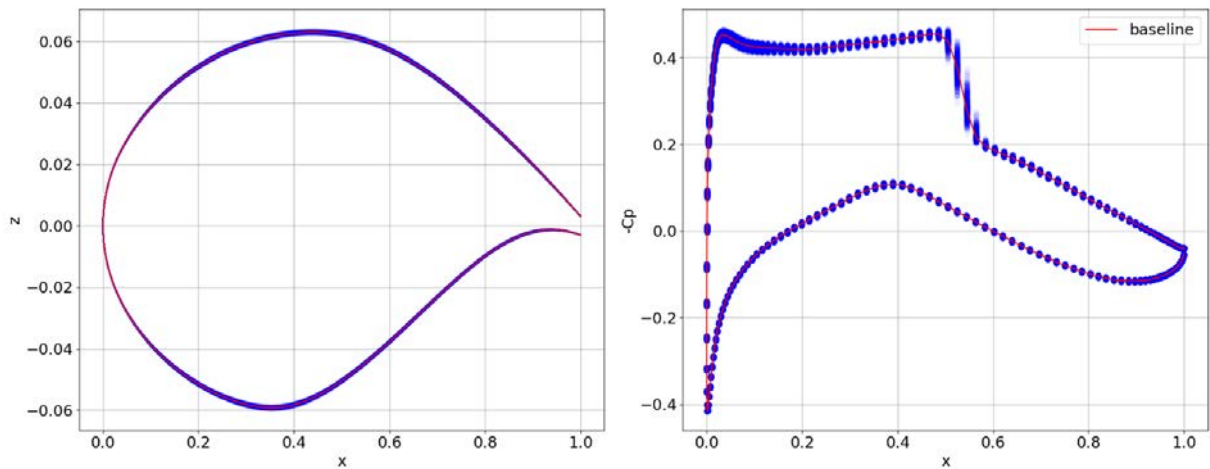Table 2: β-PDF parameters for camber and thickness uncertain design variables.

Figure 3: Airfoil shape envelope (left) and corresponding variations of the pressure coefficient distribution (right) for the DoE associated with the uncertain set Ω_1.
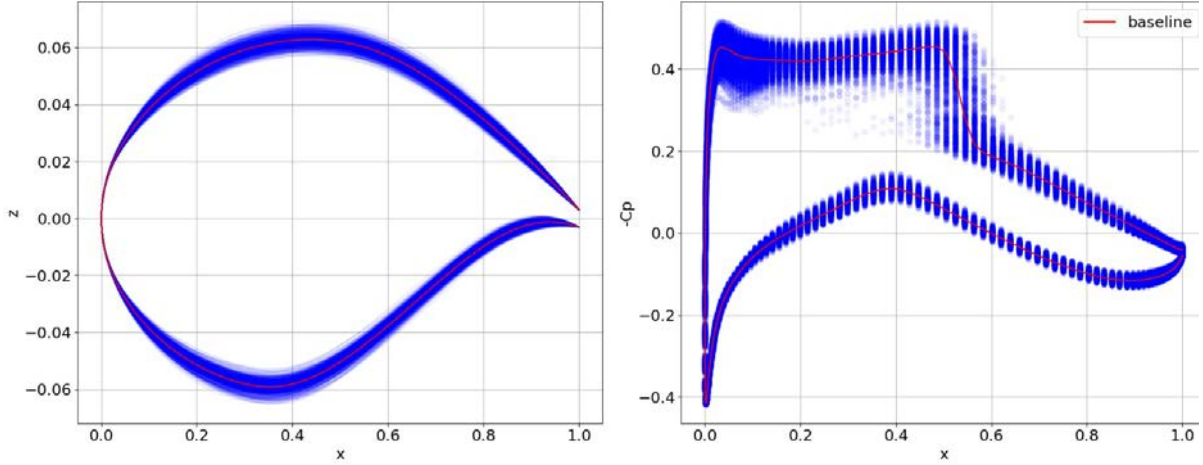
Figure 4: Airfoil shape envelope (left) and corresponding variations of the pressure coefficient distribution (right) for the DoE associated with the uncertain set Ω_2.

4 UQ RESULTS AND DISCUSSION

The comparison of UQ methods presented in this section is limited to second-order PCE approximation, as often adopted in robust optimization study for realistic applications [2]. For the considered 10 uncertain parameters, this results in a total of 66 coefficients to be computed. The standard LSA solution is employed here as a reference to asses the accuracy of the results obtained by LSA-GE, LARS and BPDN with a limited amount of data as well their potential gain in terms of efficiency. The reduced number of samples is defined as a minimum needed to attain a prescribed precision computed by the Q2 criteria. The efficiency gain is heuristically defined as the ratio between the number of samples used by LSA and their reduced number required by the other techniques, also including adjoint computations. In particular, we assume that the cost of computing a gradient for a single aerodynamic coefficient equals the one of a standard CFD run as done by [2] and [8]. However, for some complex applications, this assumption could lead to underestimate the effective cost of adjoint CFD computations, which are known to be less robust than primal ones.

For the two sets of uncertain amplitudes, Ω_1 and Ω_2, a DoE is generated using 1024 samples distributed according to a Sobol sequence. For each airfoil shape realization, a CFD evaluation of CD_{ff}, CD_w, CL, CM_y and the associated adjoint computations are carried out, resulting in a total of 5024 CFD runs. All the 1024 function evaluations are employed to feed the LSA problem. The values of mean and standard deviation estimated by using standard LSA for the different aerodynamic coefficients are reported in Table 3.

	QoI	Mean	Sigma
Ω_1	CD_{ff} (d.c.)	139.92	3.99
	CD_w (d.c.)	25.12	2.88
	CL	0.80866	6.02E-03
	CM_y	-0.09495	1.84E-03
Ω_2	CD_{ff} (d.c.)	146.80	24.49
	CD_w (d.c.)	29.97	17.32
	CL	0.80289	3.69E-02
	CM_y	-0.09481	1.13E-02

Table 3: Reference values of mean and standard deviation obtained by using standard LSA.

4.1 Mean and variance estimation

The comparison of mean and variance estimations obtained by the enhanced LSA methods for CD_{ff}, CD_w, CL and CM_y is summarized in Table 4-8, 5-9, 6-10 and 7-11, respectively. All the meta-models show very good accuracy on the mean estimations while the accuracy is reduced for the variance up to a difference of ~7% with respect to the LSA reference value. For the Ω_1 case, efficiency gains are greater for CD_{ff} and CM_y while almost halve for CD_w and CL. LARS method achieves the largest gain for each coefficient except for the wave drag. The gain is almost doubled for CD_{ff} and CL with respect to LSA-GE. BPDN achieves a performance similar to that of LARS for CD_w and CM_y. A similar behavior is also observed for the Ω_2 case, with LARS and BPDN showing a noticeably better performance than LSA-GE, with an efficiency gain which is improved by a factor ranging from ~2 up ~4 with respect to LSA-GE. The resulting PDFs are also compared in Figure 5 and Figure 6 for case Ω_1 and Ω_2, respectively. For case Ω_1 we can observe that all the PDF functions are substantially symmetric except for the pitching moment coefficient. The differences among the different methods are quite limited. The obtained best fitting using analytical PDF laws are reported in Table 8, using the Open-TURNS notation. Differently from case Ω_1, for case Ω_2 CD_{ff} and CD_w PDFs are characterized by a non-negligible skewness while those of CL and CM_y are almost symmetric as confirmed by fitting results shown in Table 13. In addition, compared to case Ω_1, larger discrepancies are observed among the different methods, especially in CD_{ff} and CD_w. For CD_w, we also observe a non-physical tail of the PDF at values lower than 0.

PCE method	Mean	Mean difference	Sigma	Sigma difference	Q2	DoE size	Performance gain
LSA-reference	139.92	-	3.99	-	-	1023	-
LSAGE	139.97	0.03%	4.21	5.51%	0.979	30	17.1
LARS	139.79	-0.09%	4.02	0.86%	0.977	33	31.0
BPDN	139.76	-0.11%	3.96	-0.84%	0.975	42	24.4

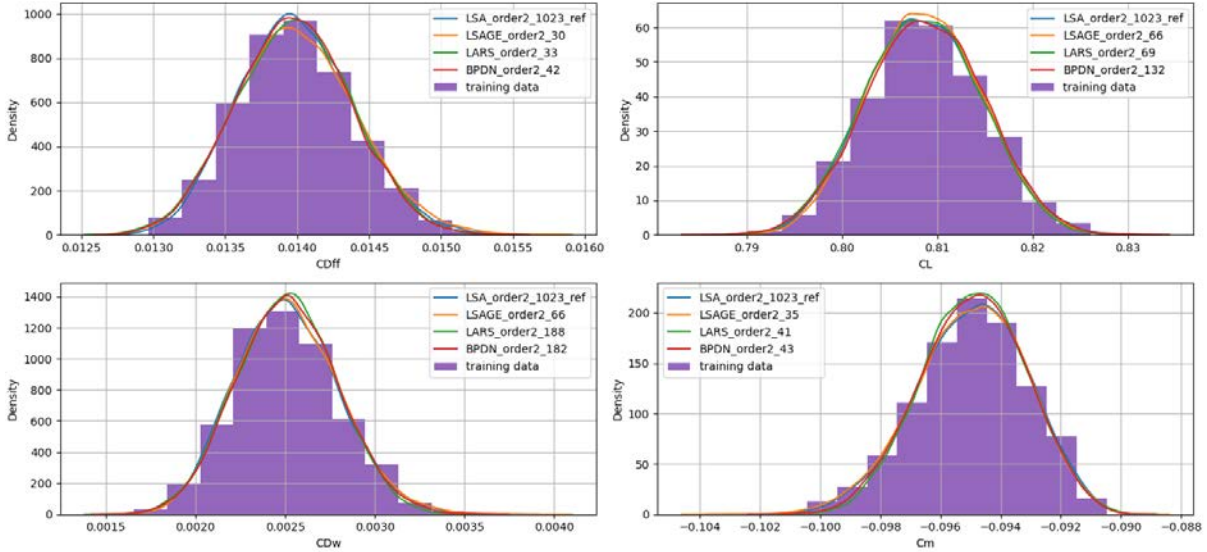Table 4: Comparison of the different methods on the estimation of the CD_{ff} statistics for uncertain set Ω_1.

PCE method	Mean	Mean difference	Sigma	Sigma difference	Q2	DoE size	Performance gain
LSA-reference	25.12	-	2.88	-	-	1023	-
LSAGE	25.18	0.25%	2.88	0.18%	0.934	66	7.8
LARS	25.07	-0.21%	2.75	-4.34%	0.926	188	5.4
BPDN	25.14	0.10%	2.81	-2.37%	0.924	182	5.6

Table 5: Comparison of the different methods on the estimation of the CD_w statistics for uncertain set Ω_1.

PCE method	Mean	Mean difference	Sigma	Sigma difference	Q2	DoE size	Performance gain
LSA-reference	0.809	-	6.02E-03	-	-	1023	-
LSAGE	0.809	0.01%	5.86E-03	-2.68%	0.958	66	7.8
LARS	0.808	-0.03%	5.98E-03	-0.66%	0.957	69	14.8
BPDN	0.809	0.01%	6.11E-03	1.48%	0.949	132	7.8

Table 6: Comparison of the different methods on the estimation of the CL statistics for uncertain set Ω_1.

PCE method	Mean	Mean difference	Sigma	Sigma difference	Q2	DoE size	Performance gain
LSA-reference	-0.095	-	1.84E-03	-	-	1023	-
LSAGE	-0.095	0.05%	1.86E-03	0.84%	0.964	35	14.6
LARS	-0.095	-0.08%	1.71E-03	-7.22%	0.963	41	25.0
BPDN	-0.095	-0.03%	1.75E-03	-5.33%	0.951	43	23.8

Table 7: Comparison of the different methods on the estimation of the CM_y statistics for uncertain set Ω_1.

Figure 5: Comparison of the histogram of the training data and the PDFs resulting from the different PCE methods for the case Ω_1.

QoI	Mean	Sigma	Skewness	Fitted PDF	Fitted PDF Parameters
CD_{ff}	139.92	3.99	0.203	LogNormal	μ =-5.23, σ=7.44e-2, γ=8.64e-3
CD_w	25.12	2.88	0.232	Dirichlet	α=[75.98, 30174.1]
CL	0.8087	6.02E-03	0.08103	Beta	α=5.51, β=5.79, a=0.79, b=0.83
CM_y	-0.09495	1.84E-03	-0.224	Beta	α=6.78, β=4.51, a=-0.103, b=-0.0897

Table 8: Parameters of the fitted distributions obtained by the LSA reference PCE method for the case Ω_1

PCE method	Mean	Mean difference	Sigma	Sigma difference	Q2	DoE size	Performance gain
LSA-reference	146.80	-	24.13	-	-	1024	-
LSAGE	146.52	-0.19%	24.45	1.29%	0.985	66	7.8
LARS	146.22	-0.40%	23.74	-1.63%	0.975	92	11.1
BPDN	146.46	-0.24%	24.24	0.45%	0.976	93	11.0

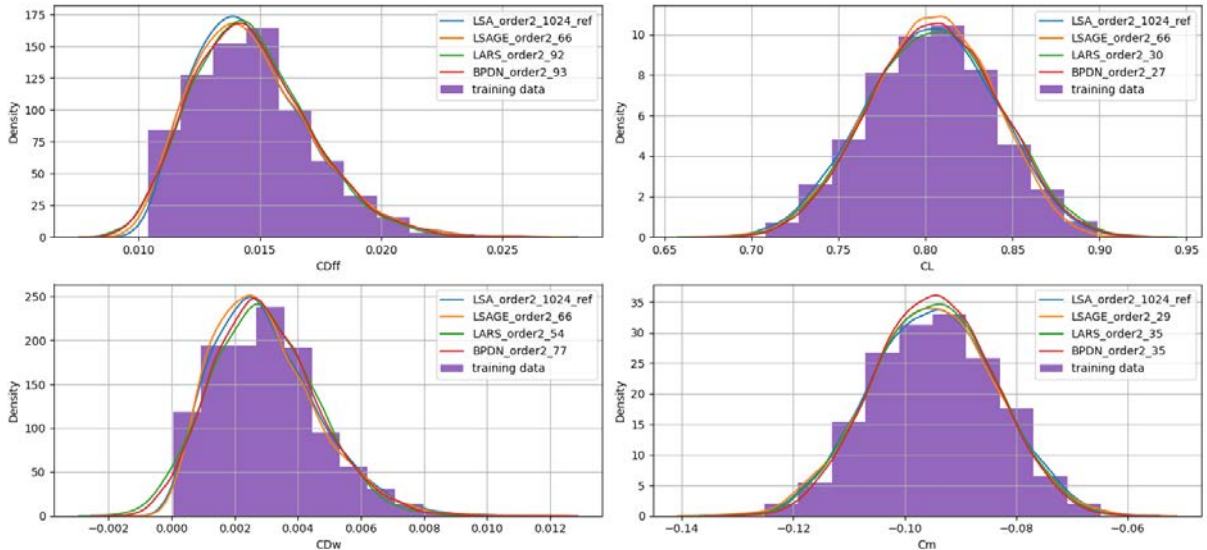Table 9: Comparison of the different methods on the estimation of the CD_{ff} statistics for uncertain set Ω_2.

PCE method	Mean	Mean difference	Sigma	Sigma difference	Q2	DoE size	Performance gain
LSA-reference	29.97	-	16.76	-	-	1024	-
LSAGE	29.50	-1.58%	16.42	-2.04%	0.939	66	7.8
LARS	29.12	-2.86%	16.48	-1.65%	0.937	54	19.0
BPDN	29.76	-0.71%	16.48	-1.65%	0.930	77	13.3

Table 10: Comparison of the different methods on the estimation of the CD_w statistics for uncertain set Ω_2.

PCE method	Mean	Mean difference	Sigma	Sigma difference	Q2	DoE size	Performance gain
LSA-reference	0.803	-	3.69E-02	-	-	1024	-
LSAGE	0.803	-0.01%	3.51E-02	-4.91%	0.965	66	7.8
LARS	0.805	0.31%	3.70E-02	0.26%	0.953	30	34.1
BPDN	0.805	0.29%	3.60E-02	-2.43%	0.954	27	37.9

Table 11: Comparison of the different methods on the estimation of the CL statistics for uncertain set Ω_2.

| PCE method	Mean	Mean difference	Sigma	Sigma difference	Q2	DoE size	Performance gain
LSA-reference	-0.095	-	1.12E-02	-	-	1024	-
LSAGE	-0.095	0.31%	1.13E-02	0.24%	0.952	29	17.7
LARS	-0.095	0.02%	1.09E-02	-2.95%	0.984	35	29.3
BPDN	-0.095	-0.05%	1.05E-02	-6.59%	0.958	35	29.3

Table 12: Comparison of the different methods on the estimation of the CM_y statistics for uncertain set Ω_2.

Figure 6: Comparison of the histogram of the training data and the PDFs resulting from the different PCE methods for the case Ω_2.

QoI	Mean	Sigma	Skewness	Fitted Distribution	Distribution Parameters
CD_{ff}	146.79	24.13	0.748	LogNormal	μ =-4.86, σ=0.295, γ=6.578e-3
CD_w	29.96	16.76	0.692	Beta	α=2.71, β=6.43, a=-4.65e-4, b=1.12e-2
CL	0.8029	3.68E-02	-0.0527	Beta	α=5.12, β=4.95, a=0.678, b=0.923
CM_y	-0.094812	1.12E-02	0.01716	Beta	α=5.53, β=5.03, a=-0.135, b=-0.0584

Table 13: Parameters of the fitted distributions obtained on the LSA reference PCE method for the case Ω_2.

4.2 Sensitivity analysis

The sensitivity analysis based on PCE first order and total Sobol indices is presented in Figure 7 and Figure 8, for case Ω_1 and Ω_2, respectively. These results indicate that the camber variable at 83% of the chord has the greatest influence on the variance of CL and CM_y while all thickness variables have a negligible effect. Conversely, for both drag coefficients, the most influent design variables are represented by thickness and camber at 17% followed by those at the 33% of the chord. A lower contribution is also observed for the camber at the 83% of the chord. All thickness variables, except the last one, show a non-negligible contribution to the variance of CD_w, which is not surprising from physical viewpoint. When analyzing interaction effects, we can observe that for case Ω_1, they are almost negligible: minor deviations of total Sobol index from first order ones are only observed for the wave drag coefficients. The differences between the considered PCE methods are also very limited. On the contrary, for case Ω_2, relevant interaction effects are observed also for the far-field drag coefficient.
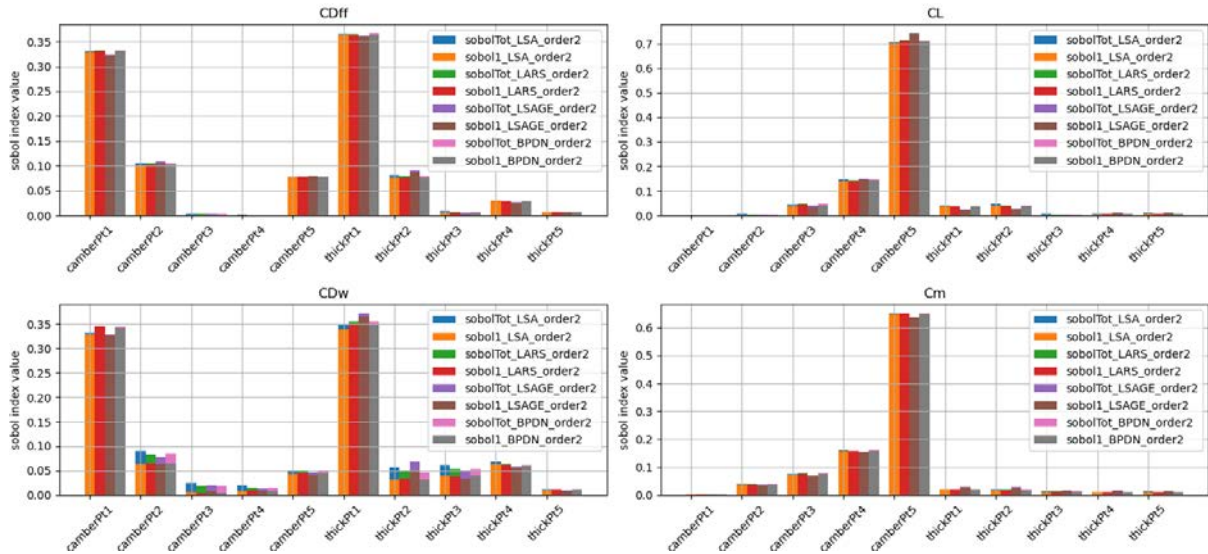
Figure 7: Comparison of the Sobol indices obtained from the different PCE methods for the case Ω_1.
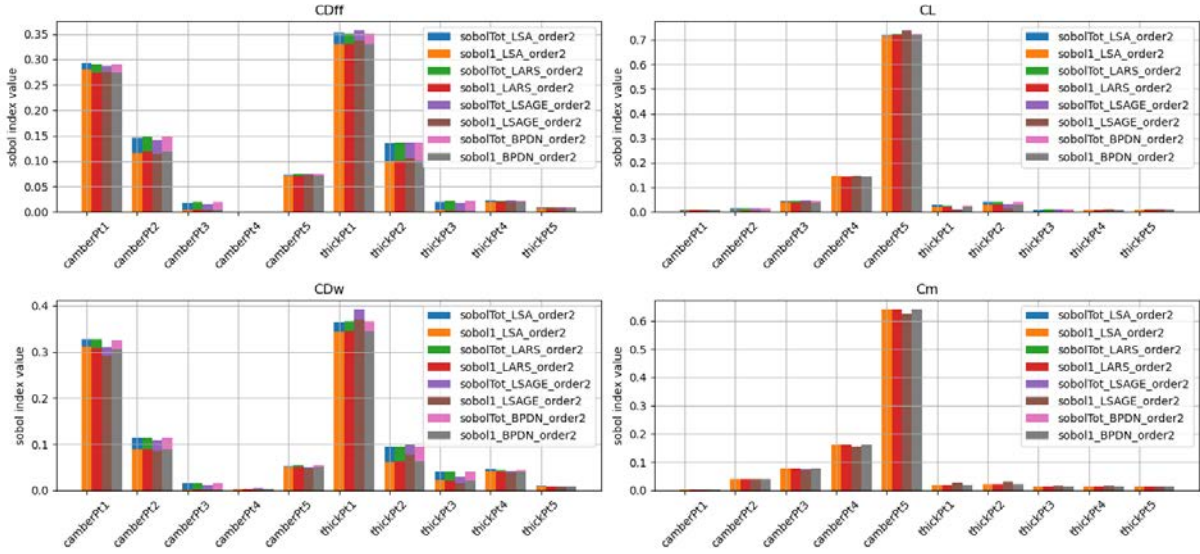
Figure 8: Comparison of the Sobol indices obtained from the different PCE methods for the case Ω_2.

5 CONCLUSIONS

This work treats two uncertainty quantification problems in dimension $d=10$. Four methods of computing a polynomial chaos expansion have been compared. The main purpose is to try to minimize the computational cost required to accurately estimate the mean and variance of four aerodynamic coefficients on a transonic airfoil. It is shown that 'gradient enhanced' and 'compress sensing' methods present significant performance gain when compared to the standard least square approximation. More precisely, the LARS method, which looks for a sparse PCE, achieve the most significant gain across all the test cases. In addition, it was found that the gain provided by LSA-GE method was sometimes lower than d, especially when dealing with larger variance of the uncertain parameter in test case Ω_2.

The achieved reduction in the size of the DoE by means of these advanced PCE techniques pave the way to a robust shape optimization using HiFi computations, building a polynomial chaos expansion at each step of the optimization. Further improvements are necessary, e.g. by combining these techniques with the dimension reduction of the uncertain design space, in order to further reduce the cost of the UQ surrogate model.

6 ACKNOLEDGMENTS

REFERENCES

[1] N. Lüthen, S. Marelli, B. Sudret, Sparse polynomial chaos expansions: Literature survey and benchmark. *SIAM/ASA Journal on Uncertainty Quantification* 9(2), 593-649, 2021.

[2] T. Ghisu, D. I. Lopez, P. Seshadri, S. Shahpar, Gradient-enhanced least-square polyno-mial chaos expansions for uncertainty quantification and robust optimization *in AIAA AVIATION 2021 FORUM (p. 3073)*.

[3] G. Blatman, B. Sudret, Adaptive sparse polynomial chaos expansion based on least angle regression. *Journal of computational Physics*, 230(6), 2345-2367, 2011.

[4] P. Seshadri, G. Parks, Effective-Quadratures (EQ): Polynomials for Computational Engi-neering Studies. *The Journal of Open Source Software* 2(11), 166, 2017.

[5] M. Baudin, A. Dutfoy, B. Iooss, A.-L. Popelin, OpenTURNS: An Industrial Software for Uncertainty Quantification in Simulation*, Handbook of Uncertainty Quantification,* Springer International Publishing, 2001-2038, 2016.

[6] L. Cambier, S. Heib, S. Plot, The Onera elsA CFD Software: Input from Research and Feedback from Industry. *Mechanics and Industry*, 14(3), 159-174, 2013

[7] D. Destarac, Drag extraction from numerical solutions to the equations of fluid dynamics: the far-field philosophy in *43ème Congrès d'Aérodynamique Appliquée de la 3AF. Maî-trise de la traînée et de l'impact sur l'environnement*, Poitiers (France), 2008.

[8] R. Mura, T. Ghisu, S. Shahpar, Least squares approximation-based polynomial chaos ex-pansion for uncertainty quantification and robust optimization in aeronautics. *In AIAA AVIATION 2020 FORUM, p. 3163, 2020.*

[9] T. Ghisu, S. Shahpar, Affordable Uncertainty Quantification for Industrial Problems: Ap-plication to Aero-Engine Fans. *ASME. J. Turbomach*, 140(6): 061005, 2018.

[10] C. Sabater, P. Bekemeyer, S. Görtz, Robust Design of Transonic Natural Laminar Flow Wings under Environmental and Operational Uncertainties, *AIAA Scitech 2021 Forum*, AIAA 2021-0071, 2021.

[11] J. Peter, F. Renac, A. Dumont, M. Méheut. Discrete adjoint method for shape optimiza-tion and mesh adaptation in the elsA code. Status and challenges. *Congrès 3AF,* Toulouse (France), 2015.

[12] S. Chen, D. Donoho, Basis pursuit. *In Proceedings of 1994 28th Asilomar Conference on Signals, Systems and Computers,* 1, 41-44, 1994.

[13] T. Gerstner, M. Griebel, Numerical integration using sparse grids, *Numerical algorithms*, 18(3-4), 209, 1998.

[14] J. Peter, Q. Bennehard. Comparison of uncertainty quantification methods for mathemat-ical problems in intermediate dimensions. *Proceedings of ECCOMAS CFD 2022*, Oslo (Norway), 2022.

[15] P. H., Cook, M. A. McDonald, C. P., Firmin M. C. P., Aerofoil RAE2822 - Pressure Distributions, and Boundary Layer and Wake Measurements, Experimental Data Base for Computer Assessment, *AGARD Advisory Report N. 138*, May 1979.